Electronic stopping power of Al_2O_3 and SiO_2 for H, He, and N

M. Peñalba,[1] J. I. Juaristi,[2] E. Zarate,[2] A. Arnau,[2,3] and P. Bauer[4,5]

[1]*Departamento de Fisica Aplicada I, ETSII T, Universidad del País Vasco/Euskal Herriko Unibertsitatea, Bilbao, Spain*

[2]*Departamento de Fisica de Materiales, Universidad del País Vasco/Euskal Herriko Unibertsitatea, San Sebastián, Spain*

[3]*Centro Mixto, CSIC–Universidad del País Vasco/Euskal Herriko Unibertsitatea, San Sebastián, Spain*

[4]*Institut für Experimentalphysik, Johannes-Kepler-Universität, Linz, Austria*

[5]*Donostia International Physics Center (DIPC), San Sebastián, Spain*

An experimental and theoretical study of the energy loss of hydrogen, helium, and nitrogen ions in alumina and silica is presented. Experimental data show that silica and alumina have a different stopping behavior. By using a model insulator dielectric function to estimate the target valence electron contribution to the stopping power, we explain the energy loss of point charges in the two oxides and extend the model to helium projectiles, where charge state effects have to be considered. At low velocities this theoretical approach shows a noticeable threshold effect related to the band gap not observed in the experiment. The low velocity data for H, He, and N ions are qualitatively explained using an electron gas model with an effective number of electrons (different for the two oxides) and a nonlinear screening description within density-functional theory. A comparison with Firsov and Lindhard-Scharf models is included for N ions as well.

PACS number(s): 34.50.Bw, 78.90.+t

I. INTRODUCTION

The electronic stopping power of light ions in heavy targets around the Bohr velocity is dominated by target valence-electron excitations. In the case of metals the free-electron-gas model has been widely used to explain the measured data [1]. In cases where screening nonlinearities are important density-functional theory has been used [2]. The basic assumption of constant density, implicit for a uniform electron gas, cannot be thought *a priori* to hold for insulators. However, recent data on the energy loss of slow ions under grazing incidence conditions on the surface of an ionic crystal (LiF) have been successfully explained using the electron-gas model with an effective valence-electron density [3]. This effective electron density was determined from the number of electrons that contribute to the stopping process.

We use a similar model to represent valence-electron excitations in the aluminum and silicon oxides and explain their different stopping behavior. Although they have similar energy gaps and valence bandwidths, they show different stopping characteristics. The orthogonalized plane-wave (OPW) model that we use explains the difference between the two oxides for point-charge projectiles. In the case of He projectiles charge-state effects have been considered in an approximate manner. Other contributions to the energy loss coming from higher-order corrections (the Barkas effect) or charge-exchange processes are not taken into account, as they are considered to be of minor importance in this case. Based on previous calculations for Al targets [4], we estimate the capture and loss processes to contribute less than 20% to the total stopping cross section for H and He projectiles. For heavier N projectiles we have compared the measured data with density-functional theory predictions for slow ions stopping and have found good agreement. The use of Firsov [5] or Lindhard-Scharff [6] models in combination with Bragg's rule [7] is also discussed. Atomic units (a.u.) will be used unless otherwise stated.

II. EXPERIMENT

In this paper we compare our theory to experimental data for H^+, He^+, and N^+ ions in Al_2O_3 and SiO_2 targets. These data were obtained in three different laboratories. Transmission data have been measured at the HMI in Berlin, by use of an electrostatic analyzer (ESA) in the energy range 15–350 keV for H^+, 35–950 keV for He^+, and 55–700 keV for N^+, using the same set of foils. The He^+ data include measurements with $^3He^+$ and $^4He^+$ isotopes; the thickness of the Berlin foils was determined by Rutherford backscattering spectroscopy (RBS) at Linz University, which also contributed to the high-energy data for protons [8]. The H^+ and He^+ data have been published in Refs. [8], [9]. For N projectiles and energies below 120 keV, the measured data were corrected for nuclear losses, by means of computer simulation using a modified version of TRIM T2D [10,11]. This correction amounted to 6% of the measured energy loss at most. These N^+ data are published in the present paper. The low-energy data for H^+ and He^+ (<15 keV) were obtained by time-of-flight spectroscopy at the IAP (Institut für Allgemeine Physik) of the Technical University in Vienna and were published in Ref. [12]. The Berlin and Vienna data are reproduced here, just to be compared to theory.

III. DESCRIPTION OF THE MODEL

A. Excitations of valence-band electrons

The contribution to the stopping power, dE/dx, of a point charge coming from the excitation of the insulator valence band is given in first order (linear-response theory) by

$$\frac{dE}{dx} = \frac{2Z_1^2}{\pi v^2} \int_0^\infty \frac{dq}{q} \int_0^{qv} d\omega\, \omega\, \mathrm{Im}\left\{\frac{-1}{\varepsilon(q,\omega)}\right\}, \quad (1)$$

where v is the ion velocity, Z_1 the ion charge, and $\varepsilon(q,\omega)$

TABLE I. Values of the parameters used to describe the modes for Al_2O_3. ω_s is the binding energy of the initial state, $1/\alpha$ the inverse of the extension of the orbital, and n is the number of electrons in this state per molecule.

Mode	ω_s (eV)	$1/\alpha$ (a.u.)	n
1	9	0.78	18
2	27.2	1.4	6

the insulator dielectric function, where q and ω are the momentum and energy transferred to the system, respectively.

In this work the OPW (orthogonalized plane wave) dielectric response function has been used [13]. This model allows us to consider different excitation modes, which are characterized by the initial state of the excited electron. In this model each mode is determined by three parameters that describe the initial state approximated by a $1s$ orbital ($e^{-r/\alpha}$): (ω_s) the binding energy, (α) the extension of the orbital, and (n) the number of electrons in the state. More precisely, for a given number N of modes,

$$\mathrm{Im}\left\{-\frac{1}{\varepsilon(q,\omega)}\right\} = \sum_{i=1}^{N} \mathrm{Im}\left\{-\frac{1}{\varepsilon_i(q,\omega)}\right\}, \qquad (2)$$

where $\varepsilon_i(q,\omega)$ is the response function corresponding to its mode, each one satisfying the first frequency moment sum rule.

The number of modes and the value of the parameters are chosen to describe the valence band of Al_2O_3 and SiO_2 in an average manner. We mean that the calculated valence-band energies and densities of states have been used to determine the value of these parameters. In the case of the Al_2O_3, band-structure calculations show that around 18 electrons per molecule (coming from the M shell of Al and the $2p$ level of O) form the valence band, and that another six electrons (coming mainly from the $2s$ level of O) form a band around 20–25 eV below the conduction band [14]. Therefore, we have considered two different excitation modes for Al_2O_3. The values used for the parameters are written in Table I.

In the case of SiO_2 12 electrons per molecule, which come from the M shell of Si and the $2p$ level of O, form two subbands, while four electrons from the $2s$ level of O are bound more or less the same as Al_2O_3 [15]. This leads us to consider three different excitation modes for SiO_2. The values of the parameters used are shown in Table II.

Concerning the energy position of the valence band for these oxides, the band-structure calculations based on the local-density approximation (LDA) of Refs. [14,15] obtain a direct band gap in the range 5–7 eV. Experimental results

TABLE II. Same as Table I for SiO_2.

Mode	ω_s (eV)	$1/\alpha$ (a.u.)	n
1	9	0.8	8
2	13.6	1.	4
3	27.2	1.4	4
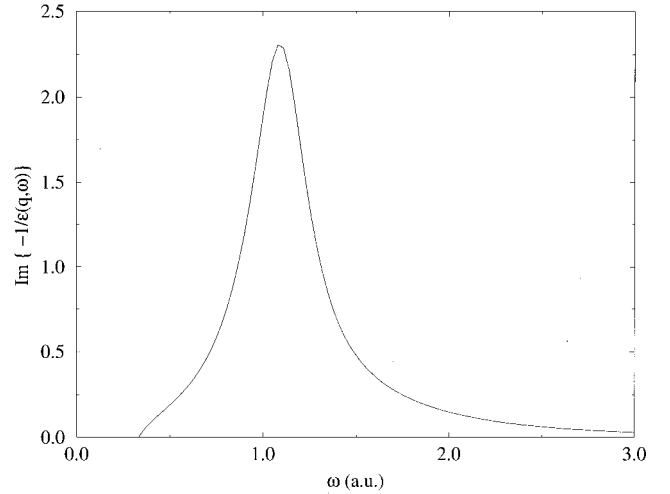
FIG. 1. OPW loss function of Al_3O_3 in the limit $q \to 0$ as a function of the energy ω.

show that the band gap is around 9 eV [16,17]. This difference is related to the underestimation of the band gap when the LDA is used. Therefore, in our model we have used the experimental value of the gap as the binding energy of the valence electrons.

In Figs. 1 and 2 the loss function ($\mathrm{Im}\{-1/[\varepsilon(q,\omega)]\}$) in the limit $q \to 0$ is plotted as a function of ω for Al_2O_3 and SiO_2, respectively. A prominent peak is observed in both cases, which corresponds to the collective (plasmon) excitation. In the case of Al_2O_3 this peak is mostly related to the 18 electrons of the valence band, whereas for SiO_2 it embodies contributions coming from the 12 electrons that form the two valence subbands.

B. Excitation of the L shell of Al and Si

In the high velocity range the contribution to the energy loss from the excitation of the L shell of Al and Si is not negligible, and therefore it has been included in the calculation. Since these electrons are strongly localized around the
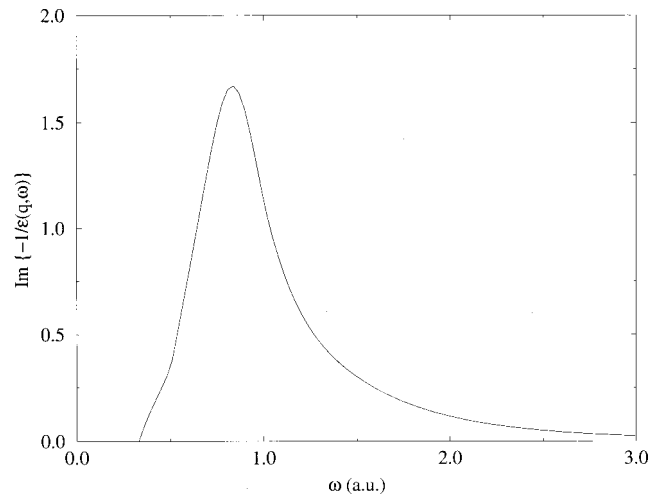
FIG. 2. Same as Fig. 1 for SiO_2.

target atoms we approximate these atomic levels and their wave functions by the values calculated for neutral atoms. Hence, in the description of these electronic levels a model approach based on the Hartree-Fock-Slater potential has been used [18]. This contribution to the stopping power is calculated in the first Born approximation for the ionization process [19].

C. Charge-state approach for He projectiles

For He projectiles in the range of velocities studied, it is necessary to consider the variation of the charge state with velocity. In this work a simple charge-state distribution has been used for singly charged ions (ϕ^+) and doubly charged ions (ϕ^{++}): $\phi^+(v) = 0.8 - 0.3(v-1)$, and $\phi^{++} = 1 - \phi^+$, based on an average of data obtained in transmission through Al foils [20]. We assume this approximation is also valid for SiO_2. This approximation is only valid in the range 1 a.u. $< v < 3$ a.u., but this velocity range comprises all the experimental data.

Since He^+ does not constitute a bare charge, Eq. (1) is modified to take into account the structure of the projectile in the following way [21]:

$$\frac{dE}{dx} = \frac{2}{\pi v^2} \int_0^\infty \frac{dq}{q} |F(q)|^2 \int_0^{qv} d\omega\, \omega\, \mathrm{Im}\left\{\frac{-1}{\varepsilon(q,\omega)}\right\}, \quad (3)$$

where $F(q) = Z_1 - \rho(q)$ (with $Z_1 = 2$ for He) and $\rho(q)$ is the Fourier transform of the projectile bound-electron charge density. The same correction is performed when calculating the energy loss originated in the ionization of the L shell.

D. Low-velocity limit

At low ion velocities ($v < 1$ a.u.) the energy-loss mechanisms in insulators are not so different from those in metals [3,12]. In the interaction of the projectile with the target atoms, molecular orbitals are formed with a subsequent reduction of the gap, which no longer affects the stopping process. Our dielectric approach is not valid at these low ion velocities, as it does not take into account nonlinear effects (such as the reduction of the gap), and therefore strongly underestimates the stopping power at these velocities. In Ref. [3] it was proposed that the electronic stopping power for ions traveling in insulators could be approximated by the value obtained using the following free-electron-gas formula:

$$\frac{dE}{dx} = v n_0 v_F \sigma_{tr}(v_F) = v Q(v_F), \quad (4)$$

where $v_F = (3\pi^2 n_0)^{1/3}$ is the Fermi velocity. The friction coefficient Q is proportional to the density of electrons (n_0) and to the transport cross section at the Fermi level (σ_{tr}) of the corresponding screened potential, which is calculated within the density-functional theory (DFT) as applied to a static impurity in an electron gas [22].

In this approach, the only parameter is the density n_0 that is determined by the number of electrons that contribute efficiently to the stopping. From the position of the plasmon
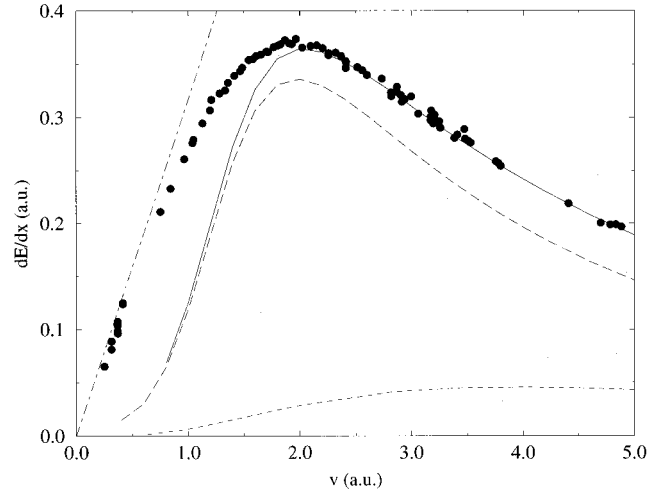
FIG. 3. Stopping power of protons in Al_2O_3 as a function of the projectile velocity. The long-dashed line is the contribution coming from the valence-band electrons calculated with the OPW dielectric response function, the short-dashed line is the contribution of the inner shells, and the solid line is the calculated total stopping power. The dashed-dotted line is the result obtained within our low velocity model. The full circles correspond to experimental data from Refs. [8,12].

peaks shown in Figs. 1 and 2 we obtain $r_s = 1.4$ a.u. for Al_2O_3 and $r_s = 1.72$ a.u. for SiO_2 where $r_s = \sqrt[3]{3/(4\pi n_0)}$.

IV. RESULTS

In Figs. 3 and 4 we show the stopping power of protons as a function of ion velocity in the range 0.4 a.u. $< v < 5$ a.u. in Al_2O_3 and SiO_2, respectively. The long-dashed line shows the theoretical calculation using linear-response theory with the OPW dielectric function. The solid line is the total stopping power when the contribution from the inner-shell excitations is also included. It is observed that inner-shell excitation contributions never exceed 20% of the total. We also show the result of our low velocity approach. Experimental
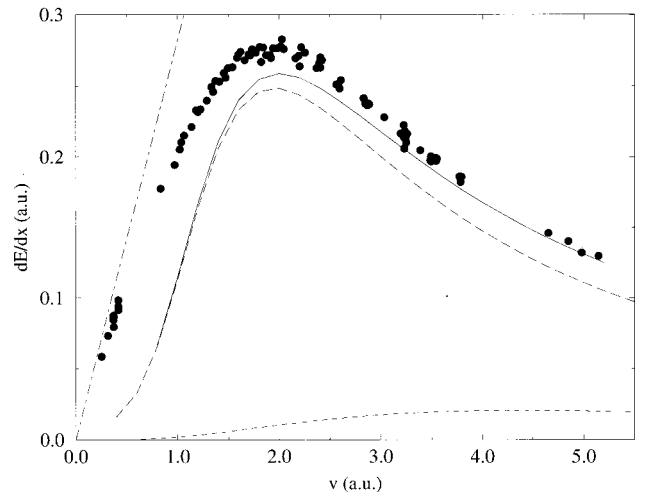
FIG. 4. Same as Fig. 3 for the SiO_2 target.
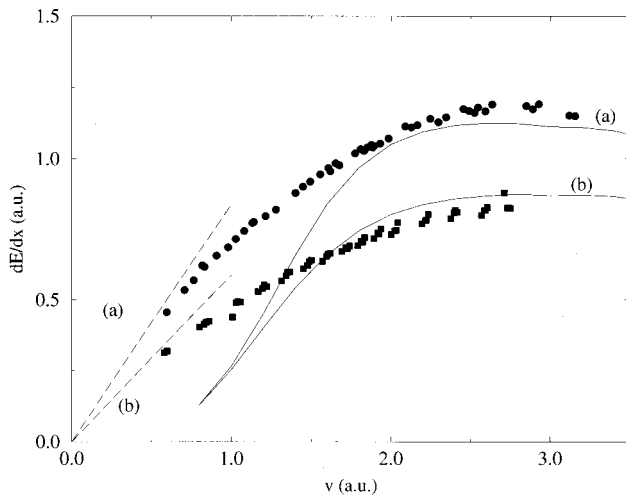
FIG. 5. Stopping power of He in Al_2O_3 and SiO_2 as a function of the projectile velocity. Solid lines are our model results obtained with the OPW dielectric response function and including the contribution of inner shells. The variation of the charge state of the ion has been taking into account (see text). Dashed lines are the results of our low-velocity model. Curves labeled (a) correspond to the Al_2O_3 target and curves labeled (c) to the SiO_2 target. The full circles and full squares correspond to the experimental data from Ref. [9] for Al_2O_3 and SiO_2, respectively.

FIG. 6. Stopping power of N in Al_2O_3 and SiO_2 as a function of the projectile velocity. The solid lines are obtained with our low-velocity model, the dashed lines with the Firsov model, and the dashed-dotted lines with the Lindhard-Scharff model. Curves labeled (a) are the results for Al_2O_3 and curves labeled (b) are the results for SiO_2. The full circles and full squares are the experimental data for Al_2O_3 and SiO_2, respectively.

values from Refs. [8], [12] are presented as well.

In the high-velocity region ($v > 2.5$ a.u.) we find a very good agreement with the experimental values. This indicates that linear-response theory is valid in this velocity regime, and that our model for the valence-band excitations is adequate to describe the energy loss in these two materials. The experimental value of the ratio of the stopping power in these materials $[(dE/dx)(Al_2O_3)/(dE/dx)(SiO_2) \approx 1.3]$ is obtained. The calculations also reproduce the position and height of the stopping maximum. At lower velocities linear-response theory does not give good agreement with the experiment due to the importance of nonlinear effects ($Z_1/v > 1$) in the energy loss. The nonlinear model based on the DFT presented above, using as density parameters $rs = 1.4$ for Al_2O_3 and $rs = 1.72$ for SiO_2, gives a much better agreement and is consistent with the approximately linear velocity dependence of the energy loss observed in the experiment. Slight deviations from linear velocity proportionality have also been observed in the stopping of H projectiles in transition metals [23].

In Fig. 5 we show our results for the stopping of alumina and silica for He ions in the velocity range 1 a.u.$< v < 3$ a.u. (from 25 to 225 keV/amu) compared with experimental data [9]. In this case the variation of the charge state has been considered. Good agreement is found between our OPW model calculations and the experimental data around and over the maximum. At low velocities the agreement is not good due to the same reasons as in the case of protons: the threshold effect in large band-gap insulators [24]. The results of the nonlinear calculation give the asymptotic behavior of the energy loss at low velocities for both oxides, using the *same* r_s values as in the case of protons.

Results for N ions are shown in Fig. 6. In this case, the experimental results correspond to the low velocities for which the dielectric approach has shown to be not valid. Therefore, in this case the nonlinear DFT method has been used to obtain the stopping powers. For both oxides good agreement is obtained with the r_s values used in this work. For comparison, results obtained using other approximations that are frequently used in the low-velocity regime as the Lindhard-Sharff and Firsov models (combined with the Bragg rule) are presented. The results obtained with the Firsov model are in good agreement with the experimental data while the Lindhard-Scharff model underestimates the energy loss. Nevertheless, the agreement obtained with the Firsov model is constrained by the limitations of the Bragg's rule that may give an overestimation of the stopping power of up to 20% [25].

V. CONCLUSION

Our model explains the stopping power of alumina and silica for protons in a wide velocity range that covers the stopping power maximum. In the case of He we find a reasonable qualitative agreement when charge-state effects are included in an approximate manner. We conclude that the OPW dielectric function is an adequate tool to describe the excitations induced by ion projectiles in the valence band of insulators at and above the stopping maximum, when band-structure information is used to describe the different modes.

At low velocities nonlinear screening effects are important: no significant threshold effect is observed in the experiment. Our low velocity model explains the measured data for H, He, and N projectiles. This shows that, as was found in a previous work for LiF [3], the energy-loss mechanisms in insulators for low-velocity ions are not so different from those in metals.

[1] P. M. Echenique, F. Flores, and R. H. Ritchie, in *Solid State Physics: Research and Applications*, edited by H. Ehrenreich and D. Turnbull (Academic, New York, 1990), Vol. 43, p. 229.

[2] P. M. Echenique, R. M. Nieminem, J. C. Ashley, and R. H. Ritchie, Phys. Rev. A **33**, 897 (1986).

[3] J. I. Juaristi, C. Auth, H. Winter, A. Arnau, K. Eder, D. Semrad, F. Aumayr, P. Bauer, and P. M. Echenique, Phys. Rev. Lett. **84**, 2124 (2000).

[4] A. Arnau, M. Peñalba, P. M. Echenique, F. Flores, and R. H. Ritchie, Phys. Rev. Lett. **65**, 1024 (1990).

[5] O. B. Firsov, Zh. Eksp. Teor. Fiz. **8**, 752 (1959) [Sov. Phys. JETP **35**, 1076 (1959)].

[6] J. Lindhard and M. Scharff, Phys. Rev. **124**, 128 (1961).

[7] W. H. Bragg and R. Kleeman, Philos. Mag. **10**, 318 (1905).

[8] P. Bauer, W. Rössler, and P. Mertens, Nucl. Instrum. Methods Phys. Res. B **69**, 64 (1992).

[9] P. Bauer, R. Golser, D. Semrad, P. Maier-Komor, F. Aumayr, and A. Arnau, Nucl. Instrum. Methods Phys. Res. B **136-138**, 103 (1998).

[10] E. Steinbauer (private communication).

[11] W. Rössler, Master thesis, University of Linz, 1992.

[12] K. Eder, D. Semrad, P. Bauer, R. Golser, P. Maier-Komor, F. Aumayr, M. Peñalba, A. Arnau, J. M. Ugalde, and P. M. Echenique, Phys. Rev. Lett. **79**, 4112 (1997).

[13] R. H. Ritchie, C. J. Tung, V. E. Anderson, and J. C. Ashley, Radiat. Res. **64**, 181 (1975); C. J. Tung, J. C. Ashley, R. D. Birkhoff, R. H. Ritchie, L. C. Emerson, and V. E. Anderson, Phys. Rev. B **16**, 3049 (1977); J. C. Ashley, C. J. Tung, and R. H. Ritchie, IEEE Trans. Nucl. Sci. **NS-25**, 1566 (1978); **NS-26**, 4874 (1979;); R. H. Ritchie, R. N. Hamm, J. E. Turner, H. A. Wright, and J. C. Ashley, Nucl. Tracks Radiat. Meas. **16**, 141 (1989).

[14] B. Holm, R. Ahuja, Y. Yourdshahyan, B. Johansson, and B. I. Lunqvist, Phys. Rev. B **59**, 12 777 (1999).

[15] Y. Xu and W. Y. Ching, Phys. Rev. B **44**, 11 048 (1991).

[16] R. H. French, J. Am. Ceram. Soc. **73**, 477 (1990).

[17] W. H. Strehlow and E. L. Cook, J. Phys. Chem. Ref. Data **2**, 163 (1973).

[18] J. P. Desclaux, Comput. Phys. Commun. **1**, 216 (1969).

[19] M. R. C. Mcdowell and J. P. Coleman, *Introduction to the Theory of Ion-Atom Collisions* (North-Holland, Amsterdam, 1970).

[20] A. Arnau, M. Peñalba, P. M. Echenique, and F. Flores, Nucl. Instrum. Methods Phys. Res. B **69**, 102 (1992).

[21] A. Arnau and P. M. Echenique, Nucl. Instrum. Methods Phys. Res. B **33**, 46 (1988).

[22] E. Zaremba, L. M. Sander, H. B. Shore, and J. H. Rose, J. Phys. F: Met. Phys. **7**, 1763 (1977).

[23] J. E. Valdes, J. C. Eckardt, G. H. Lantschner, and N. R. Arista, Phys. Rev. A **49**, 1083 (1994).

[24] D. Semrad, Phys. Rev. A **33**, 1646 (1986).

[25] D. Thwaites, Radiat. Res. **95**, 495 (1983).